Monoclinic Structured $BiVO_4$ Nanosheets: Hydrothermal Preparation, Formation Mechanism, and Coloristic and Photocatalytic Properties

Li Zhang, Dairong Chen,* and Xiuling Jiao

Department of Chemistry, Shandong University, Jinan 250100, People's Republic of China

Received: November 3, 2005; In Final Form: December 23, 2005

Bismuth vanadate ($BiVO_4$) nanosheets have been hydrothermally synthesized in the presence of sodium dodecyl benzene sulfonate (SDBS) as a morphology-directing template. The nanosheets were characterized by X-ray diffraction (XRD), field emission scanning electron microscopy (FE-SEM) equipped with an X-ray energy dispersive spectrometer (EDS), X-ray photoelectron spectroscopy (XPS), IR spectroscopy, transmission electron microscopy (TEM), and high-resolution TEM (HR-TEM). The $BiVO_4$ nanosheets had a monoclinic structure, were ca. 10−40 nm thick, and showed a preferred (010) surface orientation. The formation mechanism and the effects of reaction temperature and time on the products were investigated. UV−visible diffuse reflection spectra indicated that the $BiVO_4$ nanosheets had outstanding spectral selectivity and improved color properties compared with the corresponding bulk materials. Furthermore, the nanosheets showed good visible photocatalytic activities as determined by degradation of *N*,*N*,*N*′,*N*′-tetraethylated rhodamine (RB) under solar irradiation.

1. Introduction

In recent years, two-dimensional nanosheets or nanoplates have attracted much attention because of their unique electronic, magnetic, optical, and catalytic properties,[1] which mainly arise from their large surface areas and quantum confinement effects within the several nanometer thick sheets. A number of nanosheets made of metals,[2] metal oxides,[3] sulfides,[4] and other materials[5,6] have been prepared, and many preparative methods have been developed. These methods may be divided into two strategies: physical technologies such as thermal evaporation and physical exfoliation; and soft chemical methods such as hydrothermal/solvothermal synthesis, surfactant assistance, and use of molecular assemblies as soft templates. Although great success has been achieved in the fabrication of metal oxide nanosheets, the synthesis of multicomponent oxide nanosheets still remains a challenge. In the literature, multicomponent oxide nanosheets such as titanate and niobate nanosheets have usually been produced by exfoliating the elementary layers of layered crystals (physical exfoliation). In contrast with the number of investigations on metal, metal oxide, and sulfide nanosheets produced by soft chemical methods, few reports have appeared on the synthesis of multicomponent oxide nanosheets by these methods.[6] In fact, the soft chemical processes are complicated and some problems need to be addressed. For example, the growth mechanism of nanosheet formation from solution is not very clear, and systematic investigations on crystal growth in two dimensions are absent.

As important materials in the coatings and plastics industry, $BiVO_4$-based compounds have been extensively investigated over the past 2 decades, because they are lead-, cadmium- and chromate-free inorganic yellow pigments used to manufacture brilliant yellow shades with good gloss and hiding power.[7] $BiVO_4$ also exhibits various technological properties, such as photocatalytic activity,[8] ferroelasticity,[9] and conductivity,[10] which depend strongly on crystalline form and microstructure. $BiVO_4$ appears in three main crystalline forms: tetragonal zircon, monoclinic scheelite, and tetragonal scheelite structures. Monoclinic scheelite shows much higher photocatalytic activity under visible light irradiation and superior coloristic properties over the other forms.[8] In the literature, monoclinic micrometer-scale $BiVO_4$ powders have been prepared by solid-state reaction, solution processes, and metal organic decomposition.[11] Shantha and Varma[12] prepared nanocrystalline $BiVO_4$ particles by ball milling a mixture of bismuth and vanadium pentoxide, and Thurston et al.[13] synthesized $BiVO_4$ nanostructured powders by thermal decomposition of Bi−V bimetallic coordination complexes. Recently, Yu and Kudo[14] reported the synthesis of $BiVO_4$ nanofibers with an average diameter of 100 nm and lengths of up to several micrometers by a surfactant-assisted hydrothermal synthesis using cetyltrimethylammonium bromide (CTAB), which proved to be an effective route to control the phase structure and morphology of the products. However, production of $BiVO_4$ nanosheets has not yet been reported, to the best of our knowledge.

In this paper, a hydrothermal process that generates high-quality $BiVO_4$ nanosheets is described. $Bi(NO_3)_3{\cdot}5H_2O$ and NH_4VO_3 were used as the raw materials, and sodium dodecyl benzene sulfonate (SDBS) was used as the morphology-directing agent. As a typical soft chemical method, the hydrothermal process is promising for preparation of metal oxide nanosheets because of its many advantages. The method generates highly crystalline products, with high purity, narrow size distribution, and low aggregation. The morphology and crystal form of the products can be controlled by adjusting the hydrothermal reaction conditions. Using this method, many kinds of nanomaterials such as quantum dots (nanoparticles or nanocrystals), one-dimensional materials (nanofibers, nanobelts, nanotubes, and nanorods), two-dimensional materials (nanosheets or nanoplates), and other nanostructured materials have been prepared.[15] In the present work, we investigated the microstructure and fabrication process of $BiVO_4$ nanosheets, and elucidated the

* To whom corresponence should be addressed. Telephone: +86-0531-88364280. Fax: +86-0531-88364281. E-mail address: cdr@sdu.edu.cn.

10.1021/jp056367d CCC: $33.50
Published on Web 01/26/2006

relation of the microstructure of the nanosheets to their unique coloristic and photocatalytic properties as compared with the corresponding bulk materials.

One objective of this research is to develop a method for the fabrication of two-dimensional $BiVO_4$ nanomaterials and to investigate the formation mechanism of the nanosheets, thus enriching the available methods for preparation of muticomponent metal oxide nanosheets. The other objective is to adjust the properties of conventional functional materials by modulating the particle morphology and size of the materials, thus facilitating their development.

2. Experimental Section

2.1. Synthesis. All chemicals were analytical grade and were used as received without further purification. In a typical synthesis, 5.0 mmol (2.45 g) of $Bi(NO_3)_3{\cdot}5H_2O$ (Beijing Chemical Co.) was dissolved into 10.0 mL of 4.0 mol·dm^{-3} HNO_3 solution, while 5.0 mmol (0.58 g) of NH_4VO_3 (Shanghai Chemical Co.) was added to 10.0 mL of 2.0 mol·dm^{-3} NaOH solution. Then, 0.72 mmol (0.25 g) of SDBS (Shanghai Chemical) was added to both of the above solutions. After stirring for 0.5 h, the two solutions were mixed to give a bisque solution. The pH value of the mixed solution was adjusted to 7.0 with 2.0 mol·dm^{-3} NaOH solution, and the mixture was stirred for 0.5 h. This precursor solution was poured into a Teflon-lined stainless steel autoclave until 80% of the volume of the autoclave was occupied. The autoclave was heated at 200 °C for 1.5 h at autogenous pressure. After the autoclave was cooled to room temperature, the vivid yellow precipitate was separated by filtration, washed with distilled water and absolute alcohol several times, and then dried at 100 °C for 4 h.

2.2. Characterization. X-ray diffraction (XRD) patterns of the samples were recorded on an X-ray diffractometer (Rigaku D/Max 2200PC) with a graphite monochromator and Cu Kα radiation (λ = 0.151 48 nm) in the range of 10−80° at room temperature while the voltage and electric current were held at 40 kV and 20 mA. The morphology and microstructure of the products were determined by field emission scanning electron microscopy (FE-SEM, JEOL JSM-6700F), transmission electron microscopy (TEM, JEOL JEM-100CX) with an accelerating voltage of 80 kV, and high-resolution TEM (HR-TEM, JEOL-2010) with an accelerating voltage of 200 kV. Fourier transform infrared (FT-IR) spectra were obtained using a Nicolet 5DX Fourier transform infrared spectrometer using the KBr pellet technique in the range of 400−4000 cm^{-1}. The visible reflectance spectra were recorded on a UV−vis spectrometer (Lambda-35, Perkin-Elmer) using $BaSO_4$ as reference. X-ray photoelectron spectra (XPS) were recorded on a PHI-5300 ESCA spectrometer (Perkin-Elmer) to characterize the nanosheets' surfaces with its energy analyzer working in the pass energy mode at 35.75 eV, and the Al Kα line was used as the excitation source. The binding energy reference was taken at 284.7 eV for the C1s peak arising from surface hydrocarbons.[16] After subtraction of X-ray satellites and inelastic background (Shirley-type), peak deconvolution was carried out. Full width at half-maximum (fwhm) was kept the same for chemical components within the same core level of an element, and all component peaks were set to be Gaussian-type.

2.3. Measurements of the Coloristic Properties. $BiVO_4$ powder, varnish No. 122 (provided by Jinan printing ink factory, People's Republic of China) and kerosene were mixed according to the weight ratio of $BiVO_4$: varnish No. 122:kerosene = 4:15:1, to obtain $BiVO_4$ printing ink.[17] A paper printing sheet covered with $BiVO_4$ thin coating was prepared on a printing prototype machine. After the printing sheet was dried completely, the color data were measured with a colorimeter (TC-PΠG, Peking Optical Apparatus Factory).

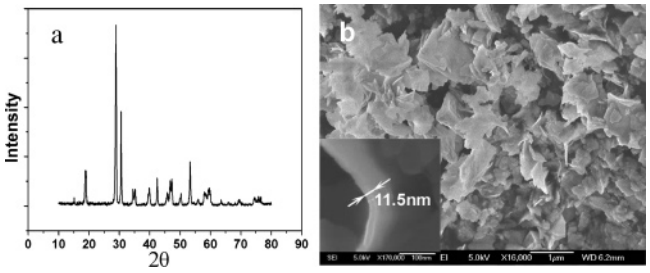

Figure 1. XRD pattern (a) and FE-SEM image (b) of $BiVO_4$ nanosheets. The inset in b is a single nanosheet standing on edge.

2.4. Measurements of the Photocatalytic Properties.[18] Photocatalytic activities of the $BiVO_4$ nanosheets were evaluated by degradation of *N*,*N*,*N*′,*N*′-tetraethylated rhodamine (RB) under the irradiation of sunlight. An aqueous $BiVO_4$ dispersion was prepared by adding 0.5 g of $BiVO_4$ powder into 100.0 mL of RB solution (2.09×10^{-4} mol·dm^{-3}). The solution was magnetically stirred and irradiated by natural sunlight. After irradiation for a designated time, the dispersion was filtered to separate the $BiVO_4$ particles, and the RB concentration of the filtrate was determined using the Lambda-35 UV−vis spectrometer.

3. Results and Discussion

3.1. Morphology and Microstructure of the Products. The XRD pattern of a typical sample (Figure 1a) indicates the nature of the phase-pure monoclinic $BiVO_4$ crystallites (JCPDS file No.14-0688). No peaks of any other phases or impurities were detected. The FE-SEM image (Figure 1b) shows that the product is well-defined nanosheets with a thickness of 10−40 nm (Figure 1b inset), in which particles with other morphologies cannot be observed. The flower pattern over the sheets is a bending contour due to the bending of the sheets (Figure 2a); this is an electron diffraction phenomenon, which is frequently observed in metal foils and other nanosheets of metal oxides.[19] The selective area electron diffraction (SAED) pattern of a single nanosheet (Figure 2a inset) shows well-defined ED spots indicating the single-crystal nature of the nanosheet, and the ED pattern can be indexed to the diffraction pattern of [010] zone axis indicating a preferred (010) surface orientation of the nanosheets.

The HR-TEM image of the nanosheets (Figure 2b) indicates their single-crystalline nature. The lattice distances of 0.3057 nm (130) and 0.3259 nm ($\bar{1}21$) and the fast Fourier transform (FFT) images (Figure 2b inset) show that the monoclinic $BiVO_4$ nanosheets have a preferred surface plane (010). However, the obvious difference in contrast and the defects at the light-colored area can be clearly observed, which might result from an oriented-attachment growth mode of the nanosheets.[20] In addition, the parallel lattice fringes changed after being irradiated by the electron beam for a few minutes, such as the area marked as a circle (Figure 2c). The changed fringes confirm that a phase transformation is occurring. The interplanar distances of 0.2991 and 0.4405 nm with the included angle of 64.08° in the changed area match well with the lattice distances of (101) and (004) in tetragonal $BiVO_4$ (JCPDS file No.83-1696), indicating a phase transformation from monoclinic $BiVO_4$ to tetrahedral $BiVO_4$. It can be observed from the insets in Figure 2b,c that the

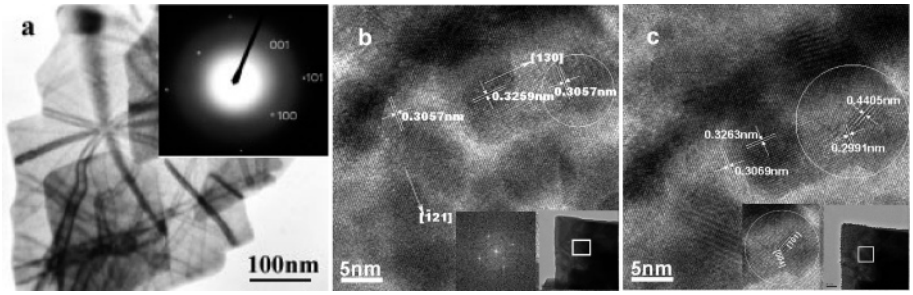

Figure 2. TEM (a) and HR-TEM (b and c) images of $BiVO_4$ nanosheets. The inset of a is the SAED pattern of a single nanosheet; the left inset in b is the FFT image, and the right one is the low-resolution TEM image of the nanosheets; and the left inset in c shows the crystal planes in the circled area, and the right one is a low-resolution TEM image of the same nanosheet.

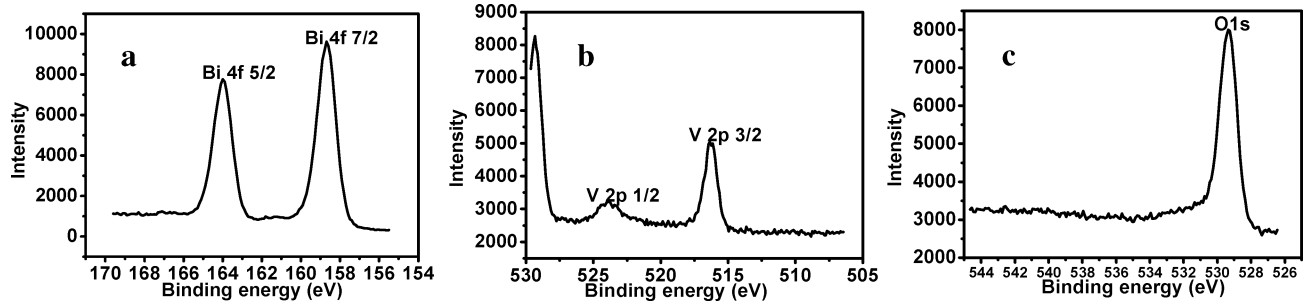

Figure 3. XPS analyses of Bi4f (a), V2p (b), and O1s (c) for $BiVO_4$ nanosheets.

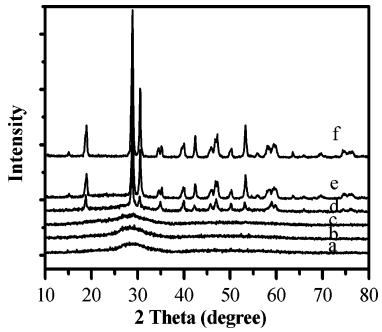

Figure 4. XRD patterns of (a) precursor and the samples after hydrothermal treatment for (b) 30, (c) 45, (d) 60, (e) 75, and (f) 120 min. Reaction temperature: 160 °C.

nanosheets become granular after 2 min of electron irradiation, which may also be attributed to the phase transformation.

The EDS analysis (the percent content of the elements (wt %): O, 17.41%; V, 10.20%; Bi, 43.34%) reveals that the elemental composition of the nanosheets is vanadium, bismuth, and oxygen with a molar ratio of Bi: V = 3.25: 3.20, which is very close to the Bi:V molar ratio (1:1) in monoclinic $BiVO_4$. The IR spectrum shown in Figure S1 (Supporting Information) shows the absorptions of $\nu_1(VO_4)$ and $\nu_3(VO_4)$ (742 cm^{-1}), weak absorptions of atmospheric CO_2 at 1634 cm^{-1} and NO_3^- anions at 1387 cm^{-1}, which are due to the absorbed CO_2 in the air and the rudimental NO_3^- anions. The XPS spectrum of the nanosheets (Figure 3) exhibits the characteristic spin−orbit split of Bi4f 5/2 and Bi4f 7/2 signals (Figure 3a), V2p 1/2 and V2p 3/2 signals (Figure 3b), and O1s peak (Figure 3c). The observed O1s peak at 529.35 eV can be assigned to the lattice oxygen in crystalline $BiVO_4$.

3.2. Formation of $BiVO_4$ Nanosheets. To investigate the formation process of $BiVO_4$ nanosheets, a detailed time course experiment was carried out. Figure 4 shows the XRD patterns of the time series samples. It can be seen that tetragonal $BiVO_4$ was formed after hydrothermal treatment for 1 h but was converted to monoclinic $BiVO_4$ as the time was prolonged to 75 min. The corresponding TEM images show that the precursor

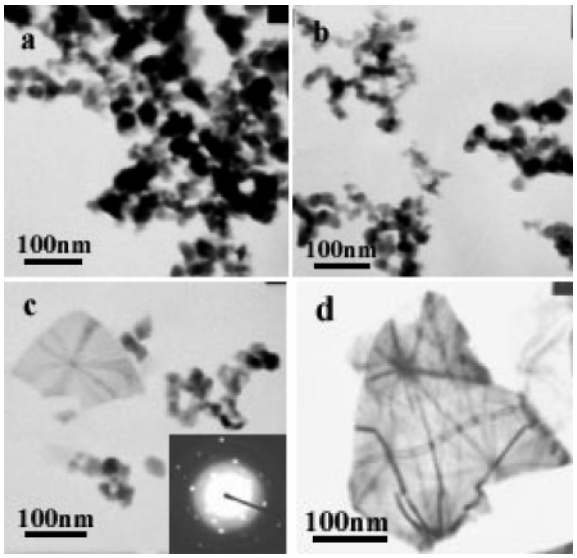

Figure 5. TEM images of (a) precursor and the samples prepared by hydrothermal treatment for (b) 45, (c) 60, and (d) 75 min. Reaction temperature: 160 °C. The inset in c is the SAED pattern of a single nanosheet.

and the samples obtained at 30 and 45 min are nanoparticles with sizes of 20−50 nm. A few nanosheets were observed in addition to the small particles in the 60 min product (Figure 5c). The ED pattern of the nanosheet (Figure 5c inset) indicates its monoclinic $BiVO_4$ nature, although the XRD pattern only shows tetragonal $BiVO_4$ peaks, which might be due to the low sensitivity of the XRD technique. The results confirm that the nanoparticles were tetragonal $BiVO_4$ and the nanosheets had a monoclinic structure. After a reaction time of 75 min, only nanosheets could be observed in the product (Figure 5d). After prolonging the treatment time to 2 h, the nanosheets grew thicker. From these phenomena, it can be concluded that the amorphous precursor first crystallized in the form of tetragonal $BiVO_4$ nanocrystals through hydrothermal dehydration, and the nanocrystals aggregated and were transformed to monoclinic

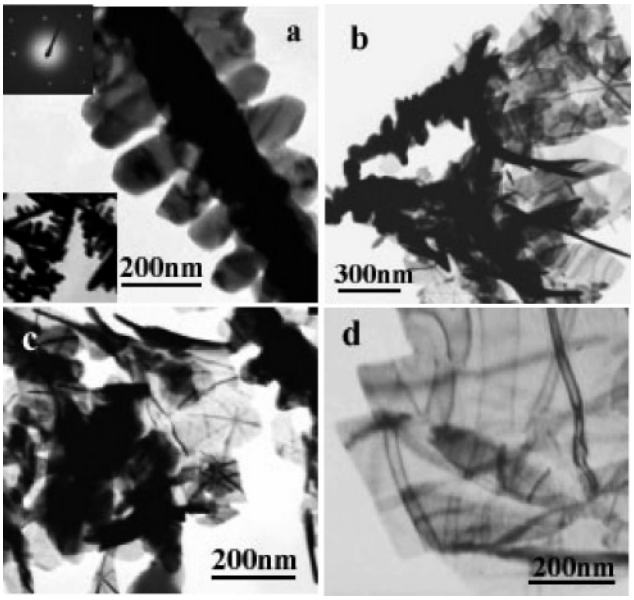

Figure 6. TEM images of products synthesized with different amounts of SDBS: (a) 0.0, (b) 0.05, (c) 0.10, and (d) 0.15 g. The top inset in a is the SAED pattern, and the lower one is a low-resolution TEM image.

nanosheets. The boundary between the aggregated nanocrystals could also be seen from the HR-TEM images (Figure 2b,c).

Control experiments indicated that the nanosheets could not form without the addition of SDBS; thus the effect of SDBS on the product was investigated. Hydrothermal experiments were conducted in the presence of different amounts of SDBS, but the reaction temperature, time, and reactant concentration were the same as those in the typical synthesis. From Figure 6, it can be seen that only fish-bone-like particles were formed in the absence of SDBS. Careful observation showed that the particles were composed of small sheetlike crystals with a thickness of 100 nm. Corresponding XRD measurements (Figure S2) indicated that the samples were all monoclinic $BiVO_4$, and the ED pattern revealed the same orientation as the nanosheets prepared in the presence of SDBS. In addition, unlike the formation of nanosheets in the presence of SDBS, there was no transformation of tetragonal $BiVO_4$ to monoclinic $BiVO_4$ during the hydrothermal process, although nanocrystals with sizes of 20−50 nm were also formed initially. With the addition of SDBS, the nanosheets appeared in the product, but more than 0.15 g of the added SDBS is necessary to obtain pure nanosheets. This is to say the formation of the nanosheets is attributed to the presence of SDBS in the present system.

As an anionic surfactant, SDBS can form micelles in aqueous solution under certain conditions, but the concentration in the present system is much lower than its critical micelle concentration (CMC). However, the ionic SDBS can be adsorbed on the surface of the $BiVO_4$ nanoparticles and affect their growth. The IR spectra of the time series samples (Figure S4 of the Supporting Information) demonstrated the existence of sulfonic radicals in the precursor compound and in the tetragonal $BiVO_4$ nanoparticles.[21] Thus, it is proposed that the adsorbed SDBS on the precursor particles favored the formation of tetrahedral $BiVO_4$ but not monoclinic particles. As to the monoclinic $BiVO_4$, the atom density on the (010) crystallographic plane is larger than those on other planes, which might provide more absorbed opportunity of the sulfonic radicals on the (010) plane. This preferred adsorption on the (010) plane further affected the aggregation of the tetragonal $BiVO_4$ nanoparticles to ultimately result in the formation of $BiVO_4$ nanosheets, accompanied by a phase transformation from tetrahedral to monoclinic $BiVO_4$. This kind of crystal formation mode assisted by organic agents is called oriented aggregation based crystal growth and has been frequently reported in recent work.[21,22] This formation mode resulted in the difference in contrast and the defects observed by HR-TEM. The small particles appearing on the surface of the nanosheets under irradiation by the electron beam resulted from a change of unit cell volume during the phase transformation and poor stability of the initial particles composing the nanosheets.

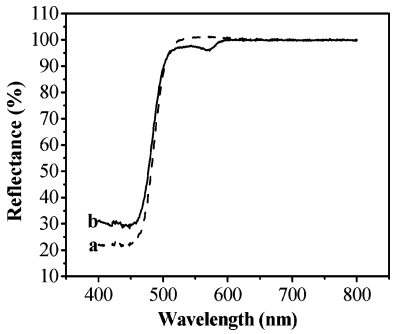

Figure 7. Reflectance curves of bismuth vanadate thin coatings: (a) nanosheets; (b) bulk materials.

3.3. Properties of $BiVO_4$ Nanosheets. *Coloristic Properties.* An important nontoxic yellow pigment, $BiVO_4$ shows different reflectances at different wavelengths: a weak reflectance at 300−450 nm and a strong reflectance in the yellow wavelengths at 500−600 nm. The better the wavelength selectivity of reflectance is, the better the pigmentary properties are.[7,17] Diffuse reflectance spectra of $BiVO_4$ thin coatings are shown in Figure 7, in which the $BiVO_4$ samples are the as-prepared nanosheets (a) and the particles shown in Figure 6a obtained in the absence of SDBS (b), respectively. The reflectance of the nanosheets in the range of 500−600 nm is higher than the nanoparticles, while that from 400 to 500 nm is significantly lower. This is to say that the spectral selectivity of the nanosheets is better than that of the powders obtained without SDBS, which means that these pigments possess good coloristic attributes.

The "Commission Internationale de l'Eclairage" (CIE) has determined standard values of L^*, a^*, and b^* that are used worldwide to measure coloristic properties, using a color measurement method called CIELAB. L^* represents the difference between light (where $L^* = 100$) and dark (where $L^* = 0$), a^* represents the difference between green ($-a^*$) and red ($+a^*$), and b^* represents the difference between yellow ($+b^*$) and blue ($-b^*$). The CIELAB system color space is shown in Figure S3 (Supporting Information).[23] The L^*, a^*, and b^* values of $BiVO_4$ thin coatings for sample A (nanosheets) on white paper were 91.64, −2.45, and 63.07, and for sample B (bulk materials) they were 91.31, 0.34, and 47.66, respectively. Sample A has larger L^* and b^* values, while its a^* value is smaller than that of sample B, which indicates that sample A gives a vivid greenish-yellow hue, while sample B gives a slightly less vivid reddish-yellow hue: furthermore the color purity and saturation of A are better than those of B. The vivid greenish yellow is an important characteristic of pure $BiVO_4$ pigment. Because the color properties depend on many factors such as chemical composition, crystal form, particle size, size distribution, and particle morphology, it is difficult to control the pigmentary colors of $BiVO_4$, and the vivid greenish-yellow hue pigment could not easily be obtained.[24] Thus the $BiVO_4$ nanosheets have improved color properties compared with the

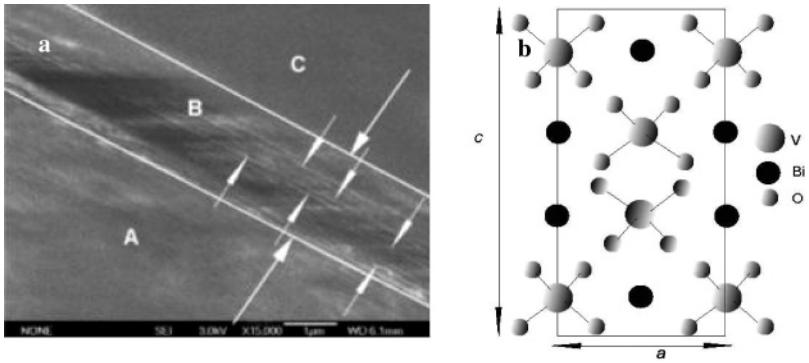

Figure 8. (a) FE-SEM pattern of a cross-section of the coating film. Section B is the coating film cross-section, section A is the paper substrate, and section C is the surface of the sample holder. (b) (010) crystal plane structure of monoclinic $BiVO_4$.

bulk material. For $BiVO_4$ pigment, the content of Bi is a crucial factor. High Bi content will contribute to the greenish yellow hue, while low Bi content will produce a paler pigment.[10] The controlled morphology of the nanosheets means that most of the exposed crystal planes are (010). The same crystal planes possess the same spectral selectivity, and this must be an important reason for the improved color properties. The FE-SEM pattern of a cross-section of the coating film (Figure 8a) shows that the $BiVO_4$ nanosheets marked with arrows are all parallel to the paper; in other words, the exposed crystal plane is the (010) plane. The corresponding (010) crystal plane structure is shown in Figure 8b. Although the nanosheets and the bulk material have the same crystal form and chemical composition, the nanosheets exposed (010) surface has a larger atom density than the (001) and (100) planes. This is likely an important reason for the improved color properties of the nanosheets as compared with the nanoparticles.

Photocatalytic Properties. Photodegradation of RB was carried out under natural sunlight. RB has a strong absorption at 552 nm, but sunlight irradiation of aqueous RB/$BiVO_4$ dispersions leads to a decrease in absorption intensity and a blue-shift of the wavelength as the RB degrades. UV−vis spectra taken over time during the photodegradation of RB mediated by $BiVO_4$ nanosheets versus bulk materials are shown in Figure 9a,b, respectively. The decrease in absorption intensity and blue-shift of the wavelength are plotted in Figure 9c,d. A control experiment on an aqueous RB solution in the absence of $BiVO_4$ powder was carried out under the same experimental conditions, but the absorption intensity and absorption wavelength hardly changed with increasing irradiation time, which is in good agreement with a previous report.[25] From Figure 9c,d it can be concluded that the degradation rate of RB mediated by nanosheets is much faster than that mediated by the bulk materials. The blue-shift of the absorption band from 552 to 539 nm arises as RB degrades into *N*,*N*,*N*′-triethylated rhodamine.[18] After irradiation for 180 min the absorption blue-shifts from 552 to 531 nm in the presence of the prepared nanosheets, indicating that RB has accomplished one de-ethylation step, while in the same time period it only blue-shifted from 552 to 549 nm using bulk materials as catalyst. The results confirm that the $BiVO_4$ nanosheets had superior photocatalytic activities compared with the bulk materials. This high photocatalytic activity must relate to the higher surface area of the nanosheets and the larger atom density of the (010) lattice plane on the exposed surfaces, which might favor the photocatylytic reaction at the surface. In addition, the photocatalytic property of monoclinic $BiVO_4$ is due to the distortion of the Bi−O polyhedron. In the present system, the thinness of the nanosheets results in a relatively large distortion of the unit cell due to the large surface strain, and the nanosheet structure means that electron−holes generated inside the crystal easily transfer to the surface and react with RB.[18] Thus, a higher photocatalytic activity was exhibited compared to the bulk material. XRD and TEM techniques are applied to check the structure and morphology of $BiVO_4$ nanosheets after photocatalytic reactions. The results (Figure S5 of the Supporting Information) indicate that no change can be detected on both the structure and morphology of the nanosheets. The photocatalytic properties of $BiVO_4$ nanosheets should have significant technical applications in solar photocatalysis.

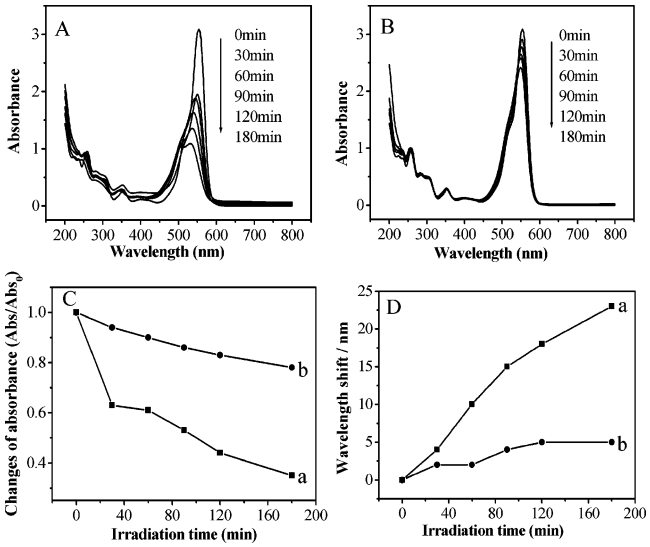

Figure 9. UV−vis spectra of RB as a function of irradiation time in the presence of the prepared $BiVO_4$ nanosheets (A) and $BiVO_4$ bulk materials (B) as catalyst. Absorbance changes (C) and wavelength shifts (D) of the major absorption using nanosheets (a) and bulk materials (b) as catalyst.

To check the differences in reactivities between the edge and the basal plane of the nanosheets, the mechanically crushed nanosheets are used as the contrastive photocatalyst. The TEM image indicates that the nanosheets have been crushed to small fragments (Figure S6 of the Supporting Information), and the edges are significantly increased. It is found that the decomposition rate of RB catalyzed by the crushed nanosheets is almost the same as that catalyzed by the noncrushed nanosheets (Figure 1b). The result reveals that the catalytic effect is mainly attributed to basal plane ((010)) of nanosheets.

4. Conclusions

In summary, $BiVO_4$ nanosheets with thicknesses of 10−40 nm were synthesized by a simple one-step route via mild

hydrothermal treatment, with the assistance of the morphology-directing agent SDBS. The formation of the nanosheets proceeds via a two-step crystallization process: first, the amorphous precursors crystallize to form tetragonal nanocrystals; then, in the presence of SDBS, the tetragonal $BiVO_4$ aggregates transform into monoclinic $BiVO_4$ nanosheets. The nanosheets are monoclinic with a preferred (010) surface. Analysis of the optical properties indicates that the pigmentary properties of the nanosheets are much better than those of the bulk materials. In addition, the nanosheets show a much higher photocatalytic activity than the bulk material for degradation of rhodamine B under solar irradiation, suggesting potential future applications in photocatalysis by sunlight.

Supporting Information Available: IR spectra of monoclinic $BiVO_4$ nanosheets and tetragonal $BiVO_4$ nanoparticles, XRD patterns of the products obtained in the presence of different amounts of SDBS, the diagram representing the CIELAB color space, and the XRD pattern and TEM image of the nanosheets after photocatalytic reactions. This material is available free of charge via the Internet at http://pubs.acs.org.

References and Notes

(1) (a) Takagaki, A.; Sugisawa, M.; Lu, D.; Kondo, J. N.; Hara, M.; Domen, K.; Hayashi, S. *J. Am. Chem. Soc.* **2003**, *125*, 5479. (b) Jiang, X. C.; Sun, L. D.; Yan, C. H. *J. Phys. Chem. B* **2004**, *108*, 3387. (c) Sakai, N.; Ebina, Y.; Takada, K.; Sasaki, T. *J. Phys. Chem. B* **2005**, *109*, 9651. (d) Chen, S. J.; Liu, Y. C.; Shao, C. L.; Mu, R.; Lu, Y. M.; Zhang, J. Y.; Shen, D. Z.; Fan, X. W. *Adv. Mater.* **2005**, *17*, 586.

(2) (a) Shirai, M.; Igeta, K.; Aria, M. *J. Phys. Chem. B* **2001**, *105*, 7211. (b) Zhu, Y. C.; Bando, Y. *Chem. Phys. Lett.* **2003**, *372*, 640. (c) Kim, J. U.; Cha, S. H.; Shin, K.; Jho, J. Y.; Lee, J. C. *Adv. Mater.* **2004**, *16*, 459. (d) Song, Y.; Yang, Y.; Medforth, C. J.; Pereira, E.; Singh, A. K.; Xu, H.; Jiang, Y.; Brinker, C. J.; Van Swol, F.; Shelnutt, J. A. *J. Am. Chem. Soc.* **2004**, *126*, 635. (e) Li, Z.; Liu, Z.; Zhang, J.; Han, B.; Du, J.; Gao, Y.; Jiang, T. *J. Phys. Chem. B.* **2005**, *109*, 14445.

(3) (a) Sasaki, T.; Watanabe, M. *J. Phys. Chem. B* **1997**, *101*, 10159. (b) Dai, Z. R.; Pan, Z. W.; Wang, Z. L. *J. Phys. Chem. B* **2002**, *106*, 902. (c) Tanaka, T.; Ebina, Y.; Takada, K.; Kurashima, K.; Sasaki, T. *Chem. Mater.* **2003**, *15*, 3564. (d) Tanaka, T.; Fukuda, K.; Ebina, Y.; Takada, K.; Sasaki, T. *Adv. Mater.* **2004**, *16*, 872. (e) Yang, X.; Makita, Y.; Liu, Z.-H.; Sakane, K.; Ooi, K. *Chem. Mater.* **2004**, *16*, 5581. (f) Fukuda, K.; Nakai, I.; Oishi, C.; Nomura, M.; Harada, M.; Ebina, Y.; Sasaki, T. *J. Phys. Chem. B.* **2004**, *108*, 13088. (g) Sakai, N.; Ebina, Y.; Takada, K.; Sasaki, T. *J. Am. Chem. Soc.* **2004**, *126*, 5851. (h) Wang, L. Z.; Sakai, N.; Ebina, Y.; Takada, K.; Sasaki, T. *Chem. Mater.* **2005**, *17*, 1352. (i) Yan, C.; Xue, D. *J. Phys. Chem. B* **2005**, *109*, 12358. (j) Mo, M.; Yu, J. C.; Zhang, L.; Li, S. K. A. *Adv. Mater.* **2005**, *17*, 756. (k) Yui, T.; Mori, Y.; Tsuchino, T.; Itoh, T.; Hattori, T.; Fukushima, Y.; Takagi, K. *Chem. Mater.* **2005**, *17*, 206. (l) Hosono, E.; Fujihara, S.; Honma, I.; Zhou, H. *Adv. Mater.* **2005**, *17*, 2091.

(4) (a) Yu, S. H.; Yoshimola, M. *Adv. Mater.* **2002**, *14*, 296. (b) Liang, C. H.; Shimizu, Y.; Sasaki, T.; Umehara, H.; Koshizaki, N. *J. Phys. Chem. B* **2004**, *108*, 9728. (c) Zhang, H.; Loh, K. P.; Sow, C. H.; Gu, H.; Su, X.; Huang, C.; Chen, Z. K. *Langmuir* **2004**, *20*, 6914. (d) Fang, X. S.; Ye, C. H.; Zhang, L. D.; Wang, Y. H.; Wu, Y. C. *Adv. Funct. Mater.* **2005**, *15*, 63;

(5) (a) Sugimoto, W.; Iwata, H.; Yasunaga, Y.; Murakami, Y.; Takasu, Y. *Angew. Chem., Int. Ed.* **2003**, *42*, 4092. (b) Liang, Z. H.; Zhu, Y. J.; Hu, X. L. *J. Phys. Chem. B* **2004**, *108*, 3488. (c) Nakano, H.; Ishii, M.; Nakamura, H. *Chem. Commun.* **2005**, *23*, 2945. (d) Wei, S.; Lu, J.; Yu, W.; Zhang, H.; Qian, Y. *Inorg. Chem.* **2005**, *44*, 3844.

(6) (a) Takagaki, A.; Yoshida, T.; Lu, D.; Kondo, J. N.; Hara, M.; Domen, K.; Hayashi, S. *J. Phys. Chem. B* **2004**, *108*, 11549. (b) Xu, F. F.; Ebina, Y.; Bando, Y.; Sasaki, T. *J. Phys. Chem. B* **2003**, *107*, 6698.

(7) Smith, H. M. *High Performance Pigments*; Wiley-VCH Verlag-GmbH: Weinheim, Germany, 2002.

(8) (a) Saimi, T.; Hideki, K.; Akihiko, K. *Chem. Mater.* **2001**, *13*, 4624. (b) Akihiko, K.; Keiko, O.; Hideki, K. *J. Am. Chem. Soc.* **1999**, *121*, 11459.

(9) (a) David, W. I. F. *J. Phys. C: Solid State Phys.* **1983**, *16*, 5093. (b) David, W. I. F.; Wood, I. G. *J. Phys. C: Solid State Phys.* **1983**, *16*, 5119. (c) David, W. I. F.; Wood, I. G. *J. Phys. C: Solid State Phys.* **1983**, *16*, 5127. (d) David, W. I. F. *J. Phys. C: Solid State Phys.* **1983**, *16*, 5149.

(10) Barreca, D.; Depero, L. E.; Noto, V. D.; Rizzi, G. A.; Sangaletti, L.; Tondello, E. *Chem. Mater.* **1999**, *11*, 255.

(11) (a) Alducci, L.; Rustioni, M. U.S. Pat. 4251283. (b) Bhattacharya, A. K.; Mallick, K. K.; Hartridge, A. *Mater. Lett.* **1997**, *30*, 7. (c) Liu, J. B.; Wang, H.; Wang, S.; Yan, H. *Mater. Sci. Eng., B* **2003**, *104*, 36. (d) Gotić, M.; Musić, S.; Ivanda, M.; Šoufek, M.; Popović, S. *J. Mol. Struct.* **2005**, *535*−*540*, 744. (e) Mara, A. B. B.; Márcia, C. N.; Carlos, P. N.; Tito, T. *Dyes Pigm.* **2005**, *65*, 125. (f) Neves, M. C.; Trindade, T. *Thin Solid Films* **2002**, *406*, 93. (g) Wood, P.; Glasser, F. P. *Ceram. Int.* **2004**, *30*, 875. (h) Galembeck, A.; Alves, O. L. *J. Mater. Sci.* **2002**, *37*, 1923.

(12) (a) Shantha, K.; Varma, K. B. R. *Mater. Sci. Eng., B* **1999**, *60*, 66. (b) Shantha, K.; Subbanna, G. N.; Varma, K. B. R. *J. Solid State Chem.* **1999**, *142*, 41.

(13) Thurston, J. H.; Ely, T. O.; Trahan, D.; Whitmire, K. H. *Chem. Mater.* **2003**, *15*, 4407.

(14) Yu, J.; Kudo, A. *Chem. Lett.* **2005**, *34*, 850.

(15) (a) Cushing, B. L.; Kolesnichenko, V. L.; O'connor, C. J. *Chem. Rev.* **2004**, *104*, 3893. (b) Rajamathi, M.; Seshadri, R. *Curr. Opin. Solid State Mater. Sci.* **2002**, *6*, 337.

(16) Schuhl, Y.; Baussart, H.; Delobel, R.; Bras, M. L.; Leroy, J. M.; Gengembre, L.; Grimblot, J. *J. Chem. Soc., Faraday Trans. 1* **1983**, *79*, 2055.

(17) Zhu, J. L. *Pigment Technology (in Chinese)*, 2nd ed.; Chemical Engineering Press: Beijing, People's Republic of China, 2002.

(18) Zhang, C.; Zhu, Y. *Chem. Mater.* **2005**, *17*, 3537.

(19) Dai, Z. R.; Pan, Z. W.; Wang, Z. L. *J. Phys. Chem. B* **2002**, *106*, 902.

(20) Hess, W. R. U.S. Pat. 4026722.

(21) He, T.; Chen, D.; Jiao, X.; Xu, Y.; Gu, Y. *Langmuir* **2004**, *20*, 8404.

(22) (a) He, T.; Chen, D.; Jiao, X. *Chem. Mater.* **2004**, *16*, 737. (b) Liu, B.; Yu, S. H.; Li, L.; Zhang, F.; Zhang, Q.; Yoshimura, M.; Shen, P. *J. Phys. Chem. B* **2004**, *108*, 2788.

(23) McLaren, K. *J. Soc. Dyers Colour.* **1976**, *92*, 338.

(24) Wood, P.; Glasser, F. P. *Ceram. Int.* **2004**, *30*, 875.

(25) Wu, T.; Liu, G.; Zhao, J. *J. Phys. Chem. B* **1998**, *102*, 5845.